Journal of the European Ceramic Society 18 (1998) 153–160

PII: S0955-2219(97)00102-7
0955-2219/98/$19.00 + 0.00

# Preparation and Properties of High Iron Oxide Content Glasses Obtained from Industrial Wastes

M. Romero and J. Ma. Rincón

The Glass-Ceramics Laboratory, Instituto E. Torroja de Ciencias de la Construcción (CSIC), Serrano Galvache s/n, 28033 Madrid, Spain

(Received 4 October 1996; revised version received 21 March 1997; accepted 18 April 1997)

***Abstract***

*The formulation and preparation of new glasses has been carried out by the recycling of goethite (FeOOH) industrial wastes originating from zinc hydrometallurgy with glass cullet and dolomite as complementary raw materials. The mineralogic (XRD) and microstructural (SEM, TEM) characterization of the product has been determined and the thermal, mechanical and chemical properties of original glasses have been measured. The results indicate that glass production is an effective recycling method for this kind of waste, yielding black stable glasses with good mechanical and chemical properties. © 1997 Elsevier Science Limited.*

***Auszug***

*Die Erstellung der Formel und Herstellung der neuen Glasarten erfolgtemittels Recycling von Goethit (FeOOH)—Industrieabfällen, welche aus der Zink—Hydrometallverarbeitung gewonnen wurden, unter Verwendung von Verpackungen aus Glas und Dolomit als Rohstoff. Es wurde sowohl eine mineralogische (XRD) als auch mikrostrukturelle (SEM, TEM) Klassifizierung vorgenommen, unter gleichzeitiger Bestimmung der thermischen, mechanischen und chemischen Eigenheiten des ursprünglich verwendeten Glases. Die erzielten Ergebnisse besagen, dass es sich bei der für die Herstellung dieser Art von Glas angewandten Technologie um eine akzeptable Form der Wiederverwendung dieser Art von Abfällen handelt, mit dem Ergebnis beständigen schwarzfarbigen Glases mit guten mechanischen und chemischen Eigenschaften.*

***Resumé***

*La formulation et l'obtention de nouveaux verres a été possible au moyen du recyclage de résidus industriels de goethite (FeOOH) obtenus de l'hydrometallurgie du zinc, en utilisant des récipients de verre et dolomite comme matières premières. On a réalisé la caractérisation minéralogique (XRD) et microstructurelle (SEM, TEM), et l'on a déterminé les propiétés thermiques, mécaniques et chimiques des verres originaux. Les résultats montrent que la technologie en vue de la production de ce type de ces résidus, permettant ainsi l'obtention de verres stables de couleur noire avec de bonnes propiétés mécaniques et chimiques.*

## 1 Introduction

In recent years there have been numerous investigations of new technologies which can reduce the harmful effects of industrial wastes in the environment. The preparation of vitreous materials technology production can be an effective route for the recycling of wastes, the production obtention and characterization of glasses from goethite (FeOOH) industrial wastes which originated in zinc hydrometallurgy have been explored previously by mixing this waste with raw materials of volcanic origin.[1,2]

A goethite waste provided by the Nuova Samín factory (Sardinia) has previously been characterized;[3] it could not be vitrified in the normal temperature range for glass production. To obtain a composition suitable for vitrification, it is necessary to mix the goethite waste with other raw materials that contain vitrifiable and fusing oxides. For economic reasons, it is also convenient to use other raw materials from industrial by-products. For this purpose a residual dolomite ($CaCO_3.MgCO_3$) from the feldspathic industry of Villavieja (Valladolid, Spain)[4] and a glass cullet have been used as complementary raw materials.

## 2 Experimental Procedure

Table 1 shows the chemical composition of the raw materials used for the glasses. From these raw materials, 11 glasses (G1–G11) have been designed with goethite content in the 30–60% by weight range. The raw materials were mixed in a ball mill for 10 min to homogenize the mixture and thus to avoid composition gradients in the melting operation. The fusion was accomplished in a superkanthal vertical electrical furnace, model SWEDISH AB pob 505, equipped with a temperature controller EUROTHERM 818 PH. For each fusion 30 g of sample was loaded in refractory silicoaluminate crucibles and introduced to the furnace at ambient temperature. The furnace was heated at 10°C $min^{-1}$ to 1450°C (melting temperature) and, with the purpose of obtaining a good homogenization of the melt, held at 1450°C for 30 min. Afterwards, the melt was cooled by pouring into brass moulds, yielding plates with dimensions $4\times4\times1\,cm^3$. To avoid possible effects of residual stresses which can affect at density, thermal and mechanical properties, the glasses were annealed at 500°C for 2 h.

## 3 Results and Discussion

### 3.1 Chemical composition

Table 2 shows the chemical analysis of the original glasses together with the theoretical composition calculated from the percentages of original raw materials (Table 1). It suggests a decrease in the content of $Fe_2O_3$, $Na_2O$ and PbO and an increase in the content of the other components, particularly in the case of $SiO_2$ and $Al_2O_3$. Taking into account that the silicoaluminous crucibles used in the fusion of these glasses contain mullite as a crystalline phase, the variations in the composition of the glasses can be explained by the different corrosion phenomena that occur during the fusion stage:

**Table 1.** Chemical analysis (wt%) of the raw materials used in glasses formulation

| | *Goethite waste* | *Glass cullet* | *Dolomite* |
|---|---|---|---|
| $SiO_2$ | 3·85 | 72·22 | 26·31 |
| $TiO_2$ | 0·06 | 0·02 | 0·26 |
| $B_2O_3$ | — | 0·02 | — |
| $Al_2O_3$ | 0·93 | 0·93 | 7·27 |
| $Fe_2O_3$ | 67·88 | 0·10 | 2·40 |
| CaO | 1·30 | 9·28 | 40·99 |
| MgO | — | 3·71 | 21·20 |
| $Na_2O$ | 0·08 | 13·45 | 0·17 |
| $K_2O$ | — | 0·09 | 1·36 |
| ZnO | 17·59 | — | — |
| PbO | 8·30 | — | — |

1. The mullite is unstable in the melted glass investigated here. With a percentage of $\approx$ 2% in alkaline oxides ($Na_2O$), the mullite can be dissociated giving rise to $Al_2O_3$ and a glass enriched in silica.[5] The combination of alkaline oxides ($Na_2O$) with the alumina derived from the dissociation of the mullite produces a sodium aluminosilicate layer at the walls of the crucible and consequently the molten glass next to the refractory is enriched in $SiO_2$ reducing at the same time its $Na_2O$ content.[6]
2. The mullite can incorporate as much as 11% of $Fe_2O_3$, with $Fe^{3+}$ ions in the octahedral and tetrahedral positions of the mullite network.[7] This incorporation produces a decrease of the $Fe_2O_3$ content in the molten glass at the same time as it increases the $SiO_2$ [8] content.
3. The decrease of the PbO content in the original glasses with respect to the theoretical composition is due to the partial volatilization of this oxide during the melting process.

### 3.2 Density

For the density measurements a Mettler 33360-210260 balance with a precision of 0.0001 g was used with water as the density fluid. The density of these materials falls in the 2·84–3·41 g $cm^{-3}$ range (Table 3). Since the density is a measurement of the degree of structural compression of the glasses,[9] the decrease in the density values observed upon reducing the $Fe_2O_3$ content in the original materials indicates an increase in the disorder of the glass network.

### 3.3 Diffraction analysis

X-ray diffraction analysis has been carried out in a Siemens Diffractometer D5000, with Cu ($K\alpha$) radiation, working at 30 mA and 50 kV with samples ground to < 37 mm. Figure 1 shows the X-ray diffractograms of the resulting materials. The G1 material shows clearly defined peaks which correspond to the crystallisation of magnetite. Therefore this material cannot be considered as a glass, but rather as having crystallised extensively in the process of cooling from the original melt. The corresponding diffractograms of G3 and G4 glassy materials show small peaks, indicating that these materials are not fully amorphous. Finally, the glasses G2 and G5–G11 do not show diffraction peaks and can be considered as non-crystalline.

### 3.4 Microstructure analysis (SEM/EDX and TEM observations)

For the microstructural study, scanning electron microscope (Zeiss DSM-950) with 20 kV acceleration voltage and with energy dispersive X-ray

**Table 2.** Chemical composition (wt%) of original glasses

| | | $SiO_2$ | $Al_2O_3$ | $Fe_2O_3$ | $CaO$ | $MgO$ | $ZnO$ | $PbO$ | $Na_2O$ | $K_2O$ |
|---|---|---|---|---|---|---|---|---|---|---|
| G1 | Theoretical | 26·74 | 1·59 | 39·62 | 7·70 | 3·23 | 11·20 | 4·44 | 4·10 | 0·20 |
| | Experimental | 38·41 | 6·42 | 29·24 | 6·63 | 2·85 | 9·47 | 2·24 | 3·92 | 0·81 |
| G2 | Theoretical | 33·56 | 1·59 | 33·07 | 8·49 | 3·60 | 9·33 | 3·70 | 5·44 | 0·21 |
| | Experimental | 43·53 | 4·68 | 25·77 | 6·99 | 3·33 | 8·34 | 1·83 | 4·83 | 0·71 |
| G3 | Theoretical | 28·97 | 2·22 | 33·30 | 11·67 | 5·35 | 9·33 | 3·70 | 4·11 | 0·33 |
| | Experimental | 40·82 | 8·10 | 25·04 | 8·65 | 3·98 | 7·33 | 1·63 | 3·56 | 0·89 |
| G4 | Theoretical | 24·38 | 2·86 | 33·53 | 14·84 | 7·10 | 9·33 | 3·70 | 2·78 | 0·46 |
| | Experimental | 39·46 | 10·80 | 23·39 | 9·46 | 4·63 | 7·02 | 1·73 | 2·54 | 0·98 |
| G5 | Theoretical | 31·19 | 2·85 | 26·98 | 15·63 | 7·47 | 7·47 | 2·96 | 4·12 | 0·46 |
| | Experimental | 42·68 | 8·04 | 20·53 | 11·24 | 5·37 | 6·15 | 1·52 | 3·61 | 0·86 |
| G6 | Theoretical | 26·60 | 3·49 | 27·22 | 18·80 | 9·22 | 7·47 | 2·96 | 2·79 | 0·59 |
| | Experimental | 41·31 | 12·42 | 18·43 | 11·54 | 5·74 | 5·55 | 1·22 | 2·59 | 1·24 |
| G7 | Theoretical | 28·82 | 4·11 | 20·90 | 22·76 | 11·34 | 5·60 | 2·22 | 2·80 | 0·72 |
| | Experimental | 37·54 | 7·60 | 18·55 | 17·50 | 8·63 | 5·29 | 1·12 | 2·85 | 0·93 |
| G8 | Theoretical | 33·41 | 3·48 | 20·67 | 19·59 | 9·59 | 5·60 | 2·22 | 4·13 | 0·59 |
| | Experimental | 41·09 | 5·08 | 18·09 | 16·52 | 7·62 | 5·14 | 1·22 | 4·52 | 0·71 |
| G9 | Theoretical | 38·00 | 2·85 | 20·44 | 16·42 | 7·84 | 5·60 | 2·22 | 5·45 | 0·46 |
| | Experimental | 44·90 | 3·63 | 18·04 | 13·99 | 6·58 | 5·27 | 1·32 | 5·68 | 0·60 |
| G10 | Theoretical | 42·60 | 2·21 | 20·21 | 13·25 | 6·09 | 5·60 | 2·22 | 6·78 | 0·34 |
| | Experimental | 50·09 | 3·65 | 16·43 | 10·75 | 5·37 | 4·97 | 1·42 | 6·69 | 0·63 |
| G11 | Theoretical | 47·19 | 1·58 | 18·98 | 10·08 | 4·35 | 5·60 | 2·22 | 8·11 | 0·21 |
| | Experimental | 53·92 | 2·11 | 15·64 | 8·80 | 4·09 | 5·05 | 1·52 | 8·43 | 0·44 |

*Iron total ($FeO + Fe_2O_3$) expressed as $Fe_2O_3$.

**Table 3.** Density of the original glasses

| | *Density (g cm$^{-3}$)* |
|---|---|
| G1 | 3·41 |
| G2 | 3·12 |
| G3 | 3·28 |
| G4 | 3·13 |
| G5 | 3·10 |
| G6 | 3·07 |
| G7 | 3·05 |
| G8 | 3·00 |
| G9 | 2·97 |
| G10 | 2·94 |
| G11 | 2·84 |

(EDX) analysis (Tracor Northem ZX-II) was used. Figure 2 is a SEM micrograph of a polished specimen of the G1 sample. It reveals a very homogeneous microstructure with all the crystallised material in the form of small rounded crystals of magnetite with $< 1\,\mu m$ size that grow to form an interconnected dendritic network. The EDX microanalysis of these crystals show a high contrast in the images obtained with secondary and backscattered electrons indicating an enrichment of the magnetite phase in $Fe_2O_3$ and of the vitreous phase in $SiO_2$.

The presence of liquid–liquid phase separation in the original glasses has been detected by TEM (Philips 300) under an acceleration voltage of 100 kV. The specimens are prepared as direct carbon replica of fresh fracture surfaces etched with HF 2% for 15s.[10] Direct observation of the glasses involved, making thin foils by ion bombardment in Gatan Dual Milling equipment, with an acceleration voltage of 6 kV and a current intensity of 20 mA, under a tilting angle of 15°.

Figure 3 shows the TEM observation of a thin foil from the G1 material. It indicates crystallisation of magnetite in the form of spherulites showing dendritic branching whose size, $\sim 0{\cdot}6\,\mu m$, corresponds to that of the small crystals which constitute the dendritic network (Fig. 2). These spherulites at the same time seem to be the clusters of nanocrystals (average dia. $< 25$ nm). Figure 3(b) shows a direct carbon replica of the same material. As expected, several dendritic growth of rounded crystals that stem from the axis of the dendrites with an angle of 90° with respect to the principal crystallisation axis. These crystals have an average size of $0{\cdot}7\,\mu m$ being formed from small nanocrystals and corresponding with the TEM observations of thin layers. In the zones between the dendrites there is a residual glass with evidence of phase separation of $\sim 60$ nm size. It is interesting to emphasize that in some zones it is possible to observe the initial stages of dendritic growth, with rounded crystal accumulations of magnetite that nucleate the dendritic growth by exsolution of iron towards the edges of the principal crystallisation axis.

The glasses have been observed by TEM for phase separation in samples prepared by the direct

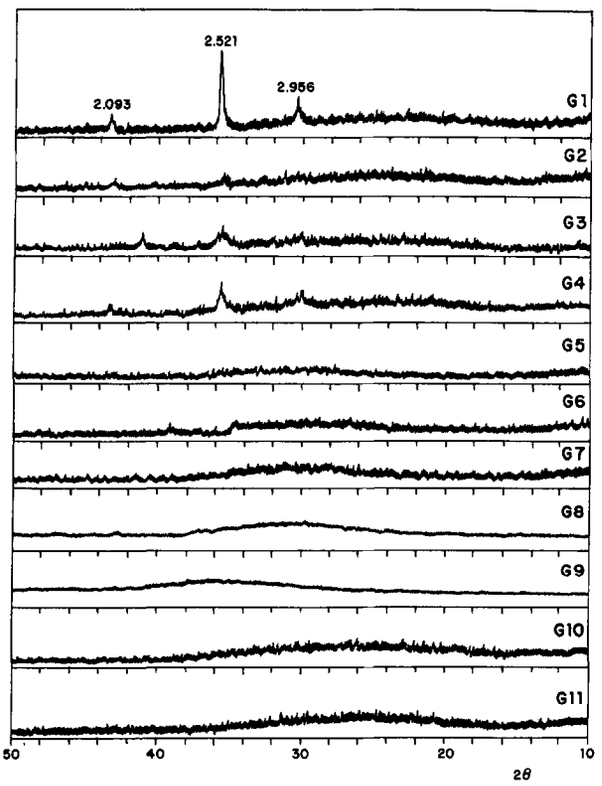


**Fig. 1.** X-ray diffractograms of original glasses.

carbon replica technique. Figure 4 shows the observations accomplished in the different glasses. The G2 glass shows phase separation 'in mosaic' with uniformly distributed drops of average size between 70–100 nm and with microcracked domains produced by gradients of expansion coefficient which are produced by the microheterogeneus character of this glass. The G3 and G4 glasses show crystallisation of dendritic type not well developed in the case of the G3 glass and polyhedric in the G4 glass. Such crystallisation should be the origin of the small diffraction peaks previously observed by XRD in these materials. In the G4 glass, near the crystallised zones, large zones of phases separation appear with average size in the 150–300 nm range.

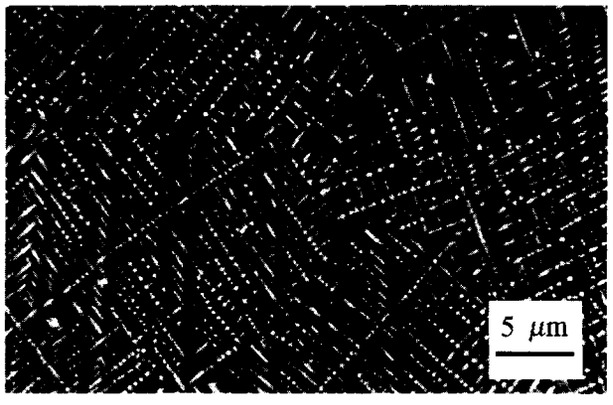


**Fig. 2.** SEM micrograph of G1 material observed by SEM in a polished sample.

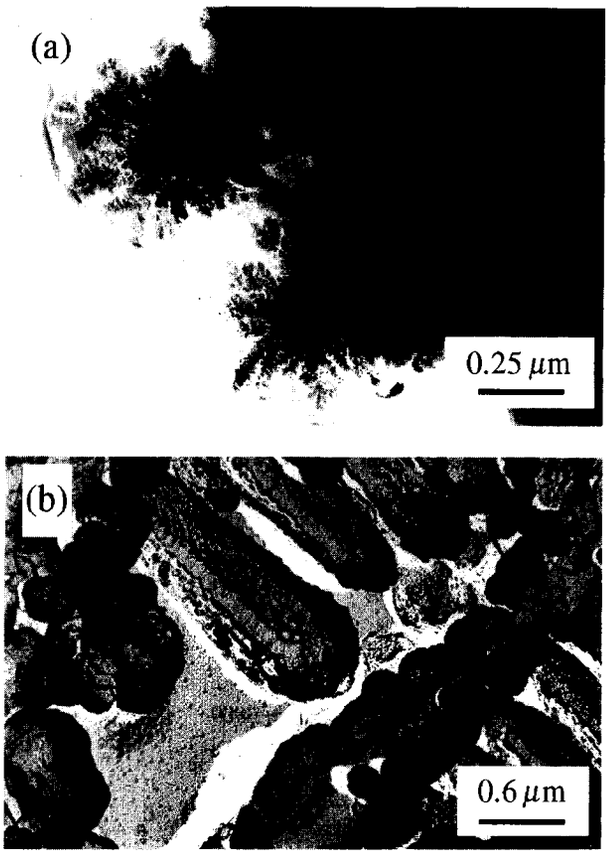


**Fig. 3.** TEM micrographs of G1 material (a) thin layer; (b) direct carbon replica from the fracture surface.

The G5 glass is clearly separated in phases, but with droplets of immiscibility of different size (130–400 μm) according to the zone that is observed. The G6 glass presents phase separation with a mean size of 300–350 nm, with droplets which are dispersed and showing high contrast with respect to the continuous glassy matrix. The G7 glass shows phase separation in mosaic with 60 μm average size and with all the areas covered with extracted particles from the fracture surface of the original glass. The G8 glass shows phase separation in the 100–200 nm range. The G9 glass is separated in phases with homogeneously distributed droplets and with two different sizes of 175 and 250 nm. Finally, the G10 and G11 glasses are phase separated with droplets of 200 nm in the G10 glass and 100 nm in the G11 the glass.

### 3.5 Differential thermal analysis (DTA)

DTA tests (Mettler TA) have been carried out in platinum crucibles by using calcined alumina as reference, in flowing air atmosphere (12 l $h^{-1}$) and with a heating rate of 10°C $min^{-1}$. Figure 5 shows the DTA curves. It is observed that all the materials show a wide exothermic band from ambient temperature to the 640–780°C interval indicating the structural reordering of the glassy network. The thermograms have different shapes for the

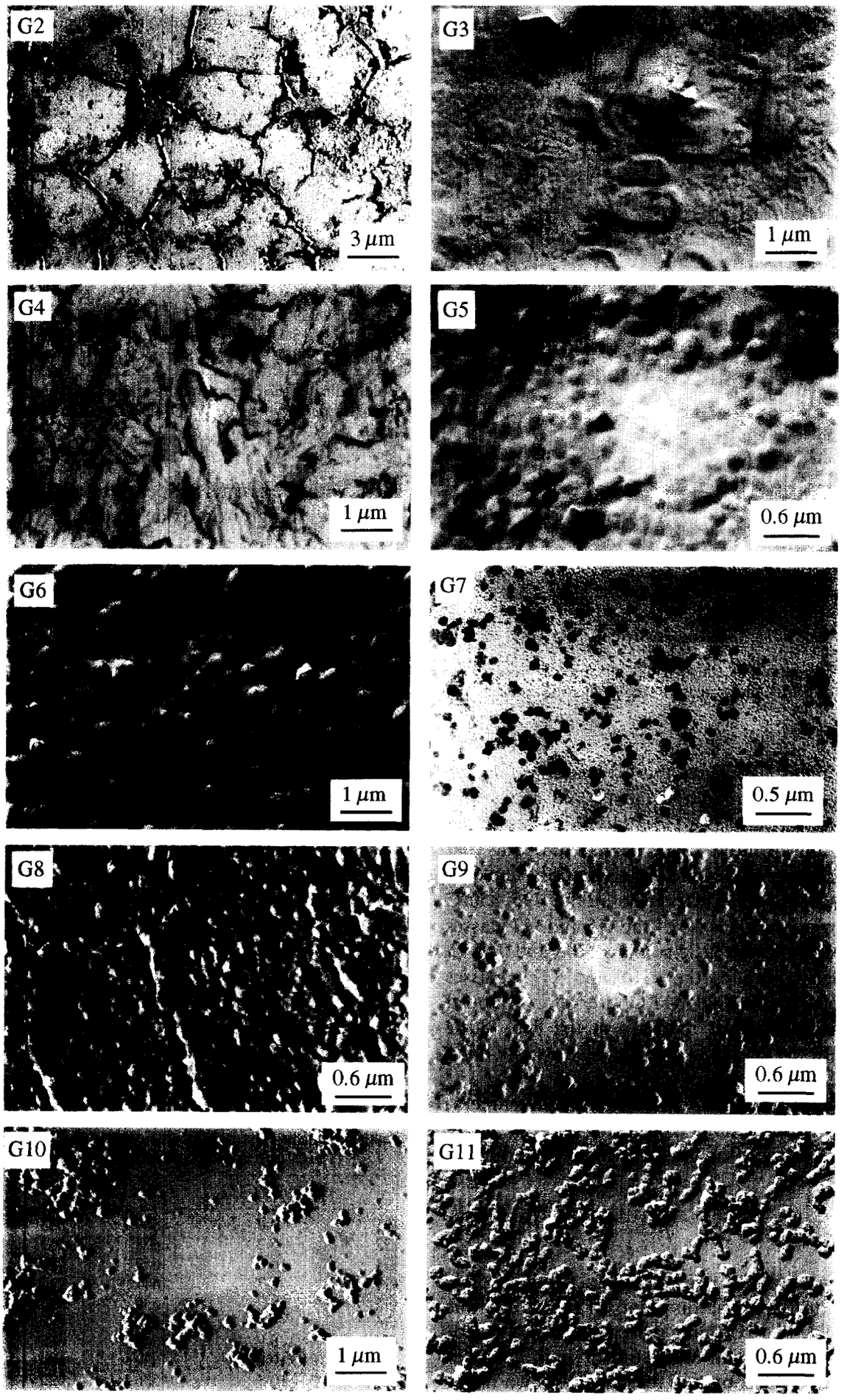


**Fig. 4.** TEM micrographs from G2–G11 glasses obtained by direct carbon replica method.

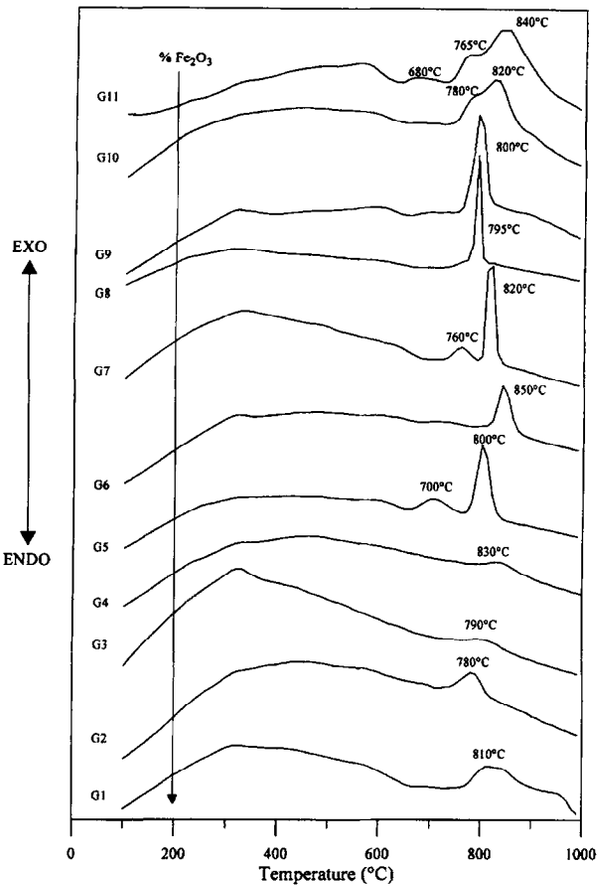


**Fig. 5.** DTA curves of the original glasses (the superposed arrow indicates the increase in the iron oxide content).

different materials. Thus, the G1 material and the G2 glass present broad and short peaks at 810 and 780°C, respectively. The G3 and G4 glasses depict thermograms without single peaks indicating that these glasses do not tend to crystallisation. The G5–G9 glasses show a clear peak in the 795–850°C interval which in the case of the G5 and G7 glasses appears close to the little peaks at 700 and 760°C, respectively. Finally, the G10 and G11 glasses show a peak in the 820–840°C interval overlapped with other of smaller intensity in the 765–780°C interval. In the G11 glass appears also a small band at 680°C.

Taking into account the exothermic temperatures and the equations from Marotta *et al.*,[11] the activation energies of crystallisation according to the expression:

$$\frac{E}{R}\left(\frac{1}{T_{f1}} - \frac{1}{T_{f2}}\right) = k$$

where $T_{f1}$ and $T_{f2}$ are the temperatures corresponding to the inflection points of the exothermic peak and $k$ is a constant whose value is 1·59 for surface crystallisation and 0·64 for bulk crystallisation. The corresponding results are shown in the Table 4. The activation energy increases in these materials for lower iron oxide content, in agreement with the greater tendency to crystallisation in glasses with high iron oxide content.

**Table 4.** Activation energy for crystallization according to Marotta *et al.* method[10]

| | $E_{act}$ *surface (kcal mol$^{-1}$)* | | $E_{act}$ *volume (kcal mol$^{-1}$)* | |
|---|---|---|---|---|
| | *Peak $I_{maximum}$ (°C)* | *2nd Peak (°C)* | *Peak $I_{maximum}$ (°C)* | *2nd Peak (°C)* |
| G1 | 47·9 | — | 19·3 | — |
| G2 | 70·6 | — | 28·4 | — |
| G3 | There are no peaks in the DTA diagram | | | |
| G4 | | | | |
| G5 | 77·0 | **186·3** | 31·0 | **75·0** |
| G6 | 198·9 | — | 80·1 | — |
| G7 | 113·3 | **188·5** | 45·6 | **75·9** |
| G8 | 359·9 | — | 144·9 | — |
| G9 | 359·9 | — | 144·9 | — |
| G10 | 115·5 | **110·3** | 46·5 | **38·6** |
| G11 | 340·2 | **78·7** | 136·9 | **31·7** |

Bold indicates the corresponding temperature to the maximum intensity peak when the ATD graph presents more than one peak.

### 3.6 Dilatometric behaviour

For the determination of the linear expansion coefficient, an Adhamel–Lhomargy DI-24 dilatometer has been used with a silicon carbide furnace and with alumina or quartz supports. The determinations have been accomplished on polished prismatic samples. The samples have been heated to 900°C at a heating rate of 10°C min$^{-1}$. Table 5 shows the values of the linear expansion coefficient ($\alpha_{20-300}$), glassy transformation temperature ($T_g$) and dilatometric softening temperature ($T_R$). In all cases, the glasses have a $T_g/T_R$ ratio in the 0·89–0·97 range. According to Uhlmann [12] the dominant nucleation mechanism for controlled devitrification would be of the heterogeneous type.

### 3.7 Mechanical properties

The microhardness has been tested by the Vickers indentation method, using a Leco microdurometer with a Vickers diamond indenter having 13° angle between faces. The samples were submitted to a

**Table 5.** Linear expansion coefficient ($\alpha$), $T_g$ and $T_R$ values for high iron content glasses here investigated

| | $\alpha(x10^6\ °C^{-1})$ | $T_g$ (°C) | $T_R$ (°C) | $T_g/T_R$ |
|---|---|---|---|---|
| G1 | 9·0 | 589 | 653 | 0·90 |
| G2 | 9·2 | 578 | 651 | 0·89 |
| G3 | 10·8 | 659 | 728 | 0·90 |
| G4 | 8·7 | 641 | 712 | 0·90 |
| G5 | 8·2 | 530 | 557 | 0·95 |
| G6 | 7·4 | 660 | 687 | 0·96 |
| G7 | 8·9 | 645 | 660 | 0·97 |
| G8 | 10·8 | 630 | 647 | 0·97 |
| G9 | 10·3 | 586 | 622 | 0·94 |
| G10 | 13·6 | 584 | 605 | 0·96 |
| G11 | 9·3 | 532 | 579 | 0·92 |

load of 1 kg for 15s. For carrying out tests to determine the Vickers microhardnes, $H_v$, and the fracture toughness or critical stress intensity factor $K_{IC}$, the elasticity modulus, $E$, (necessary for calculating the $K_{IC}$ factor) has been determined by Knoop indentation with a diamond indenter.[13,14] Table 6 shows the corresponding values, which are $E$ =83–171 GPa, $H_v$ = 5·71–6·85 GPa and $K_{IC}$ =0·83–2·02 MPam$^{1/2}$.

The material G1, with large iron oxide content, is the one which shows the best mechanical properties, possibly due to its high crystallinity resulting in an anisotropic environment for crack propagation. The Young modulus in all the cases is a greater than that of glassy silica ($E$ =71 GPa) due to the high content of $Al_2O_3$ (tetrahedrically coordinated with non-bridging oxygens) and the high CaO + MgO content (occupation of holes hindering the displacement of the Si–O–Si bonds and preventing the network deformation). In general, the Young modulus is greater than that of calcium–sodium silicate glasses ($E$ =66 GPa) and in the range of conventional glassceramics. In some cases, as in the material G1, the Young modulus exceeds that of commercial glassceramics and especially that of glassceramics of basalt type.[15]

Concerning the values of fracture toughness $K_{IC}$, these are in all cases greater than correspond to conventional glasses ($K_{IC}$ =0·6–0·9 MPam$^{1/2}$), an exception being the G2 glass. Also in the case of the material G1, the toughness value is higher than the value of fracture toughness for sintered mullite ($K_{IC}$ =1·5 MPam$^{1/2}$).

**Table 6.** $H_v$, $E$ and $K_{IC}$ of original glasses

| | $H_v$ (GPa) | $E$ (GPa) | $K_{IC}$ (MPam$^{1/2}$) |
|---|---|---|---|
| G1 | 6·85 | 171 | 2·02 |
| G2 | 6·32 | 83 | 0·83 |
| G3 | 6·01 | 137 | 1·52 |
| G4 | 6·06 | 112 | 1·15 |
| G5 | 6·43 | 106 | 1·14 |
| G6 | 6·18 | 123 | 1·52 |
| G7 | 6·26 | 107 | 1·12 |
| G8 | 6·28 | 118 | 1·17 |
| G9 | 5·94 | 122 | 1·24 |
| G10 | 6·18 | 108 | 0·94 |
| G11 | 5·71 | 91 | 0·93 |

Finally, with respect to the relative variation of mechanical properties it has been seen that, though there is not a direct relationship between the mechanical properties and the iron content in these glasses, the low values of $H_v$, $E$ and $K_{IC}$ correspond to the G10 and G11 glasses with small percentages of iron oxide.

### 3.8 Chemical properties

The effect of the high iron oxide content of the glasses on their chemical durability has been studied through hydrolytic durability on prismatic specimens tests at 70 and 90°C for 2 h. The glasses selected for this test have been the G1 and G11 materials with respectively the higher and the lower iron oxide percentages. After testing, the glasses do not show loss of weight or variation in the appearance of their surface. Table 7 shows the analytical results of leaching solutions together with the analysis of a reference solution. It has been proved that neither glass corrodes in distilled water in the conditions here used.

## 4 Conclusions

A new family of glasses with high iron oxide content has been prepared from ternary compositions based on recyled goethite and other industrial wastes. Up to a maximum of 60% incorporation of the goethite waste has been reached. The chemical composition (% wt) of the resulting glasses is: (5–10)ZnO.(3–9)MgO.(7–18)CaO.(2–12) $Al_2O_3$.(16–30)$Fe_2O_3$.(37–54) $SiO_2$. These glasses contain, furthermore, a small proportion (between 1 and 5%) of $Na_2O$, $K_2O$ and PbO.

The XRD results show that these original glasses can be classified into three groups: the G1 material has a diffractogram with clearly defined peaks indicating crystallisation of magnetite. The G3 and G4 glasses have limited structural order and the glasses G2 and G5–G11 are fully amorphous.

TEM observations samples prepared by ionic bombardment show that all the glasses are phase separated, without any relationship between the

**Table 7.** Chemical analysis in solutions obtained from water leaching ofg G1 and G11 glasses

| | Oxide ($mg^{-1}$) | | | | | | |
|---|---|---|---|---|---|---|---|
| | $SiO_2$ | $Al_2O_3$ | $Fe_2O_3$* | CaO | MgO | ZnO | PbO |
| G1 70°C/2 h | 0·59 | 0·23 | 0·13 | 0·14 | 0·02 | 0·08 | 0·05 |
| G1 90°C/2 h | 0·63 | 0·23 | 0·10 | 0·11 | 0·02 | 0·08 | 0·02 |
| G11 70°C/2 h | 0·28 | 0·05 | — | — | — | — | 0·05 |
| G11 90°C/2 h | 0·06 | 0·02 | — | — | — | — | 0·02 |
| Reference 70°C/2 h | 0·72 | 0·22 | 0·15 | 0·35 | 0·04 | 0·07 | 0·06 |
| Reference 90°C/2 h | 0·82 | 0·28 | 0·15 | 0·12 | 0·02 | 0·08 | 0·05 |

*Total iron ($Fe_2O_3$ + FeO) as $Fe_2O_3$.

size of the phase separation drops and the content of iron oxide in the glasses.

All the glasses show exothermic bands by DTA in the 680–850°C interval, with activation energy of surface crystallisation in the 48–360 kcal $mol^{-1}$ range and activation energy of bulk crystallisation in the 19–145 kcal $mol^{-1}$ range. With $T_g/T_R$ =0·89–0·97, crystallisation nucleation of these glasses must take place by heterogeneous nucleation.

The high iron content glasses depict $H_v$, $E$ and $K_{IC}$ higher than those of commercial conventional glasses. The glasses are chemically inert in water.

From the results of this investigation, it can be concluded that vitrification is an effective way for recycling industrial wastes such as the goethite red muds, giving rise to stable glasses with good mechanical and chemical properties which could be used as decorative tiles or pavements in construction purposes.

## Acknowledgement

The authors thank the European Union (European Project RAW MATERIALS-DG XII (MA 2R CT90-0007)) for the financial support of this work.

## References

1. Pelino, M., Cantalini, C., Boattini, P. P., Abbruzzese, C., Rincón, J. Ma. and García-Hernández, J. E., Glass-ceramic materials obtained by recycling goethite industrial wastes. *Resources, Conservation and Recycling*, 1994, **10**, 171–176.
2. Romero, M., Rincón, J. Ma., Cantalini, C. and Pelino, M., Properties and applications of high iron content glass-ceramics obtained from recycling of goethite wastes. In *Ceramics: Charting the Future*, ed. P. Vicenzini, Techna Srl, Florence, 1995, pp. 229–236.
3. Romero, M., Procesado y caracterización de nuevos vidrios y materiales vitrocerámicos obtenidos por reciclado de residuos industriales de goethita. Ph.D. thesis, Universidad de Alcalá de Henares, Facultad de Ciencias Químicas, Madrid, 1995.
4. Ibañez, A., Vicente, A. P., González-Peña, J. Ma. and Sandoval, F., Utilización de una marga dolomítica en la obtención de chamotas anortítica y diopsido-wollastonítica. *Bol. Soc. Esp. Ceram. Vidr.*, 1990, **29**(1), 5–8.
5. Pena, P., Refractarios para zonas de contacto con el vidrio. *Bol. Soc. Esp. Ceram. Vidr.*, 1989, **28**(2), 89–96.
6. Carlos Fueyo, D. J., Puntos débiles del refractario en los hornos de vidrio: Posibles líneas de solución. *Bol. Soc. Esp. Ceram. Vidr.*, 1989, **28**(2), 97–103.
7. Schneider, H. and Rager, H., Iron incorporation in mullite. *Ceramics International*, 1986, **12**, 117–125.
8. Schneider, H., Iron exchange processes between mullite and coexisting silicate melts at high temperatures. *Glastechnologie Ber.*, 1989, **62**(6), 193–198.
9. Fernández Navarro, J. M., *El Vidrio*, Consejo Superior de Investigaciones Científicas, Madrid, 1991.
10. Bradley, T., Uses of carbon replicas in elecron microscopy. *Journal of Applied Physics*, 1956, **27**, 1399–1412.
11. Marotta, A., Saiello, S., Branda, F. and Buri, A., Activation energy for the crystallisation of glass from the DDTA curves. *Journal of Materials Science*, 1982, **17**, 105–108.
12. Uhlmann, D. R., A kinetic treatment of glass formation. *Journal of Non-Crystalline Solids*, 1972, **7**, 337–348.
13. Marshall, D. B., Tatsuo, N. and Evans, A. G., A simpled method for determining elastic modulus to hardness ratios using Knoop indentation measurements. *Journal of the American Ceramic Society*, 1982, **10**, 175–176.
14. Rincón, J. Ma. and Capel, F., Microstructure behaviour $K_{IC}$ factor determination and microstructure analysis of some $Li_2O$-$SiO_2$ glass ceramics materials. *Ceramics International*, 1985, **71**, 97–102.
15. Strnad, Z., *Glass-Ceramics*, Elsevier, Amsterdam, 1990.